*Chinese Science Bulletin* 2006 Vol. 51 No. 18 2281—2286

**DOI: 10.1007/s11434-006-2090-4**

# Analysis on contact and flow features in CMP process

ZHANG Chaohui[1], LUO Jianbin[2], LIU Jinquan[1] & DU Yongping[1]

1. School of Mechanical, Electronic and Control Engineering, Beijing Jiaotong University, Beijing 100044, China;
2. State Key Laboratory of Tribology, Tsinghua University, Beijing 100084, China

Correspondence should be addressed to Zhang Chaohui (email: zhangchaohui@tsinghua.org.cn)

Received January 17, 2006; accepted June 12, 2006

**Abstract** Contact pressure and flow features of chemical mechanical polishing/planarization (CMP) process were analyzed, taking advantage of the one-dimensional contact model of two layers and considering slurry flows. In this model, deformations of the bulk pad substrate and the asperities were considered. The deformations of the bulk pad substrate and the asperity layer, as well as the contact pressure and fluid pressure, were revealed with numerical methods. Numerical simulation results show a counterintuitive phenomenon: a diverging clearance is formed in the leading region of the wafer and thereby it gives rise to a suction pressure (subambient pressure). A high stress concentration is presented at the wafer edge and thereby over polishing can be introduced. The research provides some theoretical explanations for these two fundamental features of usual CMP processes.

**Keywords: chemical mechanical polishing, contact stress, subambient fluid pressure.**

Chemical mechanical polishing/ planarization (CMP) has evolved into a key technology of integrated circuit (IC) industry to accomplish wafer surface polishing with high precision[1]. To a larger extent, however, CMP is still a black art, i.e. empirical or semi-empirical data are of urgent necessity to optimize the parameters in an attempt to achieve ideal polishing outcomes[2]. This limits the possible uses of the technology[3].

During CMP processes, a rotating wafer to be polished is pressed face-down onto a rotating resilient pad, while the slurry, usually containing abrasive particles and chemical reagents, flows in between the wafer and the pad. Thus CMP possesses complex tribological behaviors, including chemical reaction and mechanical effects. Most of the slurries contain silica-based nanoscale particles, whose inner motions make contributions to the surface quality of the wafer to be polished afterwards[4,5].

The pad is the key component of CMP, which plays a crucial role in both mechanical and chemical polishing process[6]. It can carry the slurries, water and chemical reagents onto the wafer surface, and deliver byproducts in CMP process (such as waste polishing slurries). In the meantime, the pad can provide partial mechanical actions in CMP process (for instance, it can make direct contact with the wafer surface), and can provide suitable chemical and mechanical environment.

The pad surface is usually made rough enough and therein pores are fabricated to facilitate debris delivery. By and large, a harder pad is conducive to planarity promotion, while a soft polishing pad improves global planarization and formation of defect-free wafer surface.

Levert *et al.*[7] pointed out that there was commonly a subambient fluid pressure (a suction pressure to the wafer) in the system consisting of wafer, pad and slurries, and typical mean suction pressure was well below the vapor suction pressure. Tichy *et al.*[8] proposed a preliminary elastic model for the contact mechanics and fluid mechanics to account for this finding. The assumptions in the analysis were rather simple, thus affecting the precision and credibility of the model predictions. The present paper addresses the contact and flow relations of CMP by modification.

## 1 Model description

The one-dimensional contact model, incorporating slurry flows considered here is schematically shown in Fig. 1. The pad surface is very rough by usual tribology standards, and it is resilient. It is regarded as composed of two layers: one is the bulk pad substrate and the other is the asperity layer. In Fig. 1, the asperity height is denoted by the average mean value. These two layers have different elastic responses while undergoing pressure. The wafer will have a displacement under exerted outer load, which is composed of the deformations of the asperity layer and the bulk pad substrate layer. To simplify this problem, the following assumptions are introduced.

(i) The wafer is rigid enough, and the deformations (including those of the bulk pad substrate and the rough asperities) are purely elastic (neglecting, in fact, the plastic deformations accompanying the CMP process).

(ii) The calculation of the elastic deformation of the

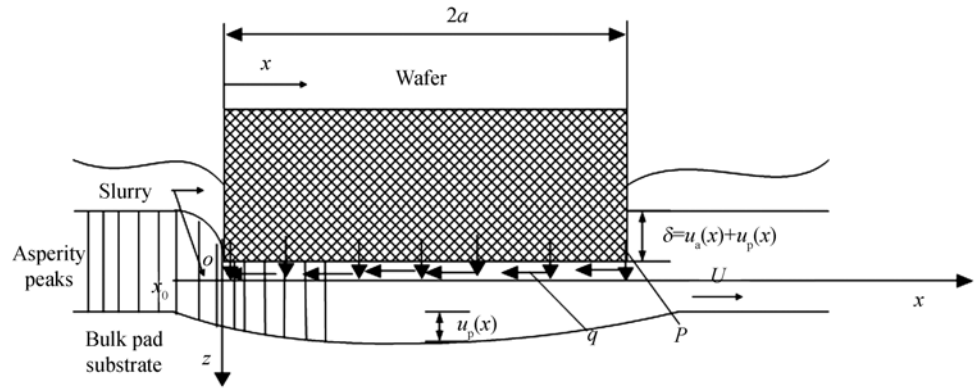


Fig. 1. Schematic of analysis model.

bulk pad substrate is taken from a classic formula of contact with a semi-infinite medium. The pad thickness used is usually about 1 mm, while the deflection of the pad substrate is usually of the order of several microns. So this assumption is creditable.

(iii) The load exerted is balanced by the solid contact pressure of the deformed asperities and the fluid pressure of the slurry fluids. The flow of the slurry is considered as one-dimensional.

(iv) The slurry fluids flow through a film of elastically deformed compressed asperities, whose height is essentially the effective one of the averaged compressed asperities.

(v) The fluids of the slurry are looked upon as behaving in a Newtonian viscous manner. The slurry usually contains nano-scale solid particles or gels, which are microstructures but contributes little to the flow features due to the small size of the particles and the relatively small fraction. The effects of microstructure are neglected here.

The deflection of the bulk pad substrate are computed with classical semi-infinite formula, while the deflection of the asperities are calculated with Mattress model assuming that the asperities are deformed independently each other[9], in which the local displacement is only affected by the local normal pressure, and the shear stress has no influence on the asperity normal displacement.

$$u_p(x)=\frac{2(1-\nu^2)}{\pi E}\int_0^{2a} p_s(s)\ln\left|\frac{x-s}{x_0-s}\right|ds + \frac{(1-2\nu)(1+\nu)}{2E}\left(\int_0^x q(s)ds-\int_x^{2a} q(s)ds\right) + \frac{(1-2\nu)(1+\nu)}{2E}\left(-\int_0^a q(s)ds+\int_a^{2a} q(s)ds\right), \quad (1)$$

$$u_a(x)=\frac{p_s(x)}{K}, \quad (2)$$

where $\nu$ is Poisson's ratio; $E$ is the elastic modulus of the bulk pad substrate; $a$ is the radius of the wafer; $p_s$ is the solid contact pressure; $q$ is the surface shear stress (it is assumed to have no effect on asperity deformation); and $K$ is the effective elastic constant. The subscript p denotes the bulk pad substrate and the subscript a denotes asperity layer. Both of them support the same solid contact pressure.

$x$-direction takes the flow direction of the slurries, and it is zero at the leading edge. $x_0$ is the position with zero deformation of the bulk pad substrate in the absence of shear stress, which is always taken as indefinite in the theoretical sense. By eq. (1), the value of the moment at the wafer center resulting from shear stress is zero. These two assumptions are improvements of that in ref. [8]. Similarly, to simplify the calculation, the surface shear is assumed to be uniformly distributed over the whole surface, and the value is $q_0$. The wafer is regarded as with no tilting.

The mean normal load is calculated by

$$\frac{\int_0^{2a}(p_s+p_f)dx}{2a}=p_{app}, \quad (3)$$

where $p_{app}$ is the applied mean load, and $p_f$ is fluid pressure.

In the absence of normal load, the rigid wafer rests on the asperity tips and the equivalent film thickness, which equals the undeformed effective asperity height, is denoted by $h_0$. From geometry relation (Fig. 1), one can get

$$h_0=\delta+h(x)-u_p(x) = h(x)+u_a(x), \quad (4)$$

where $\delta$ is the deflection of the wafer, and $h(x)$ is the

equivalent fluid film thickness of the slurries.

It follows from eq. (4) that

$$\delta = u_a(x) + u_p(x). \tag{5}$$

Summarizing the aforementioned relations, the following deflection relation can be deduced:

$$\delta + \frac{(1-2\nu)(1+\nu)}{E} q_0(x-a) = \frac{p_s(x)}{K} - 2\frac{(1-\nu^2)}{\pi E}\int_0^{2a} p_s(x)\ln\left|\frac{x-s}{x_0-s}\right| ds. \tag{6}$$

In the case of static loading without shear stress, eq. (6) reduces to

$$\delta = \frac{p_s(x)}{K} - 2\frac{(1-\nu^2)}{\pi E}\int_0^{2a} p_s(x)\ln\left|\frac{x-s}{x_0-s}\right| ds. \tag{7}$$

Eqs. (6) and (7) are integrals with respect to unknown $p_s(x)$, which can be solved by iteration methods.

Assuming that the fluid pressure obeys the Reynolds equation and that the fluids are taken as one-dimensional incompressible Newtonian fluids, the following relation holds:

$$\frac{d}{dx}\left(h^3 \frac{dp_f}{dx}\right) = 6\eta U \frac{dh}{dx}, \tag{8}$$

where

$$h(x) = h_0 - \frac{p_s(x)}{K}. \tag{9}$$

## 2 Numerical procedures

### 2.1 The calculation of the integral

The integral of eq. (6) or (7) can be calculated after discretization.

$$I(x_i) = \int_0^{2a} p_s(s)\ln|x_i - s|\,ds = \sum_{j=1}^{N} C_{ij} p_s(x_j), \tag{10}$$

$$C_{ij} = (i-j+0.5)\Delta\left(\ln(|i-j+0.5|\Delta) - 1\right) - (i-j-0.5)\Delta\left(\ln(|i-j-0.5|\Delta) - 1\right), \tag{11}$$

where $i$ and $j$ are discretized nodes, $N$ is the number of nodes, and $\Delta$ is the step length ($\Delta = 2a/N$).

### 2.2 Distribution relaxation

We can solve eqs. (6) and (7) by relaxation methods. Because any alternation at a given point will change the elastic deformations of all other points, relaxations either based on Gauss-Seidel method or on Jacobi scheme may not converge steadily. The calculation scheme on the basis of distributive relaxation[10] should be adopted to confine the alternations in elastic deformation resulting from the change in pressure to a minimum. That is, different from usual relaxation scheme, wherein one only applies change to pressure at node $i$, pressures at nodes $i$ and $i$–1 ($\delta_i$ and $-\delta_i$ are added) are modified to satisfy the discretized equation.

### 2.3 Numerical simulation procedure description

The numerical calculation procedure can be briefly described as follows. Firstly, the overall elastic deformation $\delta$ (i.e. the rigid displacement of the wafer) is supposed. Then the solid contact pressure $p_s$ are computed from the discretization of eq. (6). Subsequently $u_p$ and $u_a$ are obtained. The fluid pressure $p_f$ are calculated from eq. (9). According to the differences between the exerted load and the summation of the solid contact pressure and the fluid pressure, the elastic deformation is modified in advance. Repeat these steps to attain a convergence solution (balanced load relation) and then halt the procedure.

## 3 Numerical simulation results

### 3.1 Static loading case

Parameters used in computation procedure are adopted as follows: elastic modulus of the bulk pad substrate $E$ = 40 MPa, Poisson's ratio of the pad $\nu$ = 0.4, and wafer half-length $a$ = 0.05 m. The elastic constant of asperity layer is $K = 5.0\times10^9$ Pa/m, and the total elastic displacement is set at $\delta$ = 40 μm. Eq. (7) is then solved according to the procedure described above.

Fig. 2 gives the comparison of the effects of the choices at the position of zero displacement (variant $x_0$). The solid line expresses the computing results with $x_0$ = 0 (the same as that in ref. [8]), while the dashed line denotes the case of $x_0 = -5a$. It can be seen that the computed solid pressure with $x_0$ = 0 is much larger, almost doubled. According to elastic theories, $x_0$ represents the integral constant, and should be taken as infinitive. In practical computation procedures, one can use $x_0 = -5a$ to attain precise solution (which is used hereinafter in computation).

Fig. 3 shows the influences of elastic constant on computed static contact pressure. As is evident in the figure, there exists high stress concentration near the boundaries, which is magnified for the nearly rigid case. In the center of the contact, the increase of the contact pressure is relatively small.

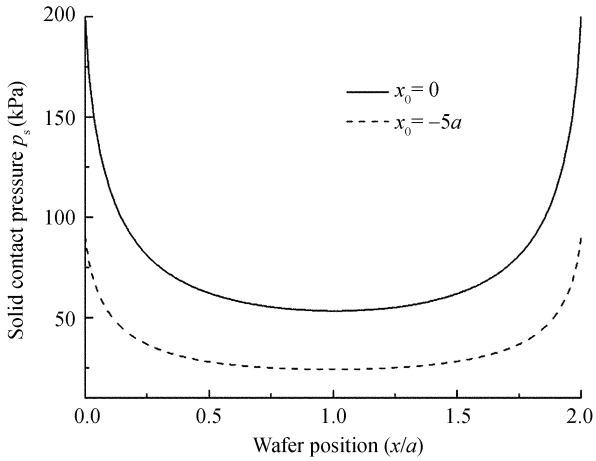


Fig. 2. Effects of zero displacement point on pressure at static contact.

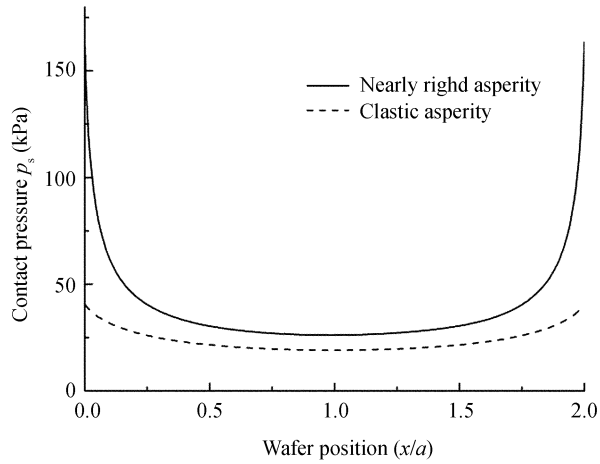


Fig. 3. Influences of the elastic constant of asperity on computed static contact pressure. Elastic case: $K = 1.5\times10^9$ Pa/m; nearly rigid case: $K = 1.5\times10^{10}$ Pa/m.

The corresponding deflections of the bulk pad substrate and the asperities are shown in Figs. (4) and (5), respectively. Fig. 4 shows the elastic case with $K = 1.5\times10^9$ Pa/m, while Fig. 5 shows the nearly rigid case with $K = 1.5\times10^{10}$ Pa/m. Note that the limitation of $\delta = u_a(x) + u_p(x)$ is set. When the asperity is softer (Fig. 4), the deflections of the bulk pad substrate and the asperity layer are nearly the same, whereas for the nearly rigid case (Fig. 5), the deflections are mainly due to the bulk pad substrate. Furthermore, the softer asperities will result in larger diverging region that will subsequently give rise to larger fluid suction force. This is in good agreement with experimental results of Levert *et al.*[7].

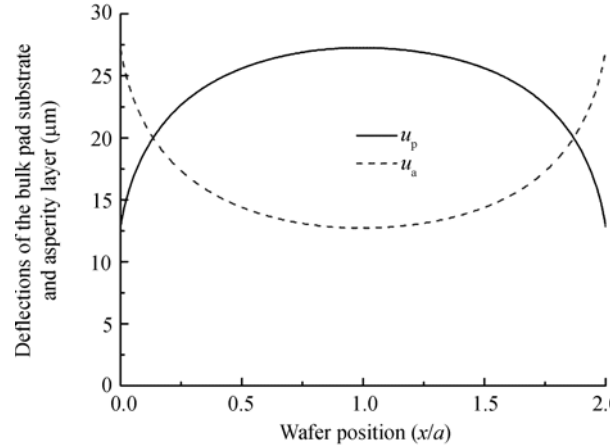


Fig. 4. Deflection of elastic asperities ($K = 1.5\times10^9$ Pa/m).

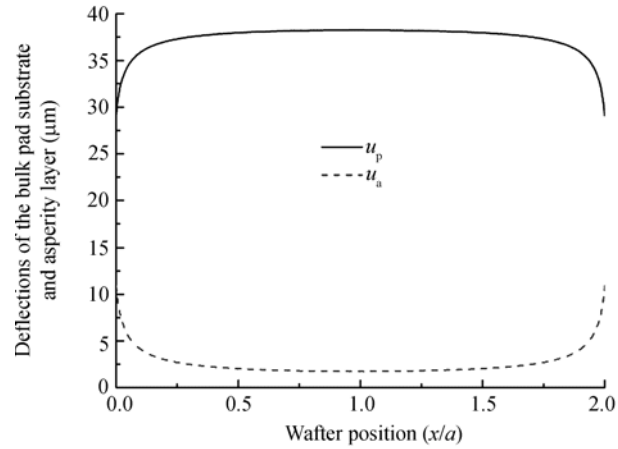


Fig. 5. Deflection of nearly rigid case ($K = 1.5\times10^{10}$ Pa/m).

### 3.2 *Sliding case*

Parameters different from those in static case are: mean exerted outer load $p_{app}$ = 25 kPa, friction shear stress $q$ = 10 kPa (with a typical friction coefficient of 0.4), viscosity of slurry $\eta$ = 0.0025 Pa·s and velocity $U$ = 0.4 m/s. The elastic constant of asperity layer is $K = 2.5\times10^9$ Pa/m. The equivalent height of the asperity layer without applied load is set at 65 μm.

Fig. 6 shows the simulated contact pressure. Due to the existence of frictional shear stress, the solid contact pressure is no longer symmetric about the center (refer to Figs. 2 and 3). High stress concentration also appears at the edges while it keeps nearly stable in central span. The mean solid contact pressure is about 26 kPa.

The deflections of the bulk pad substrate and the asperities are shown in Fig. 7. Similarly, due to friction shear stress, they are not symmetric with the center po-

sition by which a larger diverging region (refer to Fig. 8) is thus formed in the leading edge facilitating the subambient pressure formation of the slurry fluids.

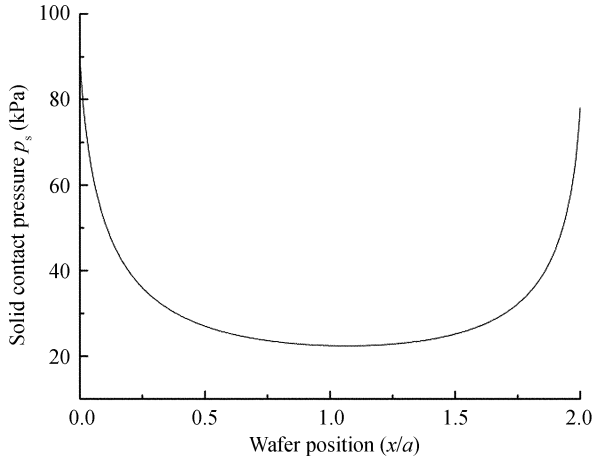


Fig. 6. Contact pressure with sliding.

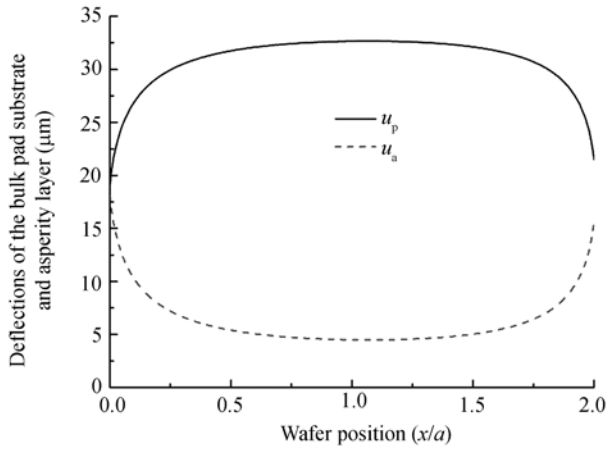


Fig. 7. Deflections of the bulk pad substrate and asperity in sliding case.

Fig. 8 shows the distribution of slurry film thickness from computation, whose corresponding fluid pressure is elucidated in Fig. 9. The film thickness at the leading edge is smaller than that at the trailing edge. A diverging region is thus formed in the leading edge, which ensures the formation of subambient pressure. Due to frictional shear stress, the diverging region at the leading edge is larger than the converging region at the trailing edge, where the larger region of subambient pressure comes. The computed maximum subambient pressure is about −50 kPa, and the mean fluid pressure is about −1.06 kPa. This value is larger than that measured in experiments. It is likely that the effects of the asperities are over magnified. Otherwise, it may be due to the ignoring of the porous property of the pad (the subambient pressure can be compensated by the fluids flow through the pores). The actual factors remain to be further explored.

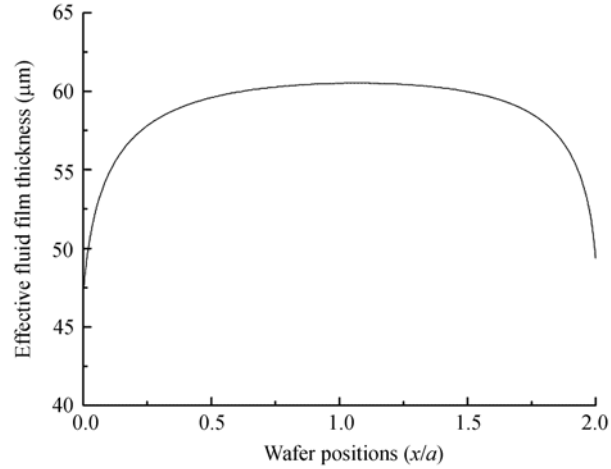


Fig. 8. Distribution of the slurry clearance.

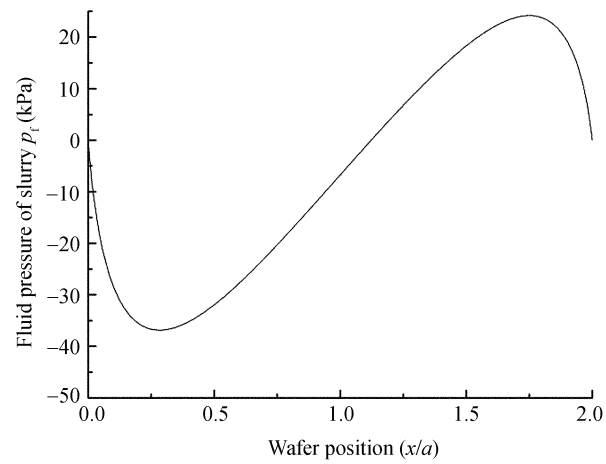


Fig. 9. Fluid pressure of slurry.

Fig. 10 shows the total pressure distribution. High stress concentrations appear at edges and the pressure drops fast at the leading region. Subambient pressure region may thus take place. It should be noted that the total high stress concentration at edges will accelerate wear process and thereby lead to over polishing. So the polishing quality is deteriorated (practically, an over polished region is usually fabricated and should be avoided[11]). Thus decrease in stress concentration at edges and uniformed pressure in contact region are of great importance in improving the polishing quality.

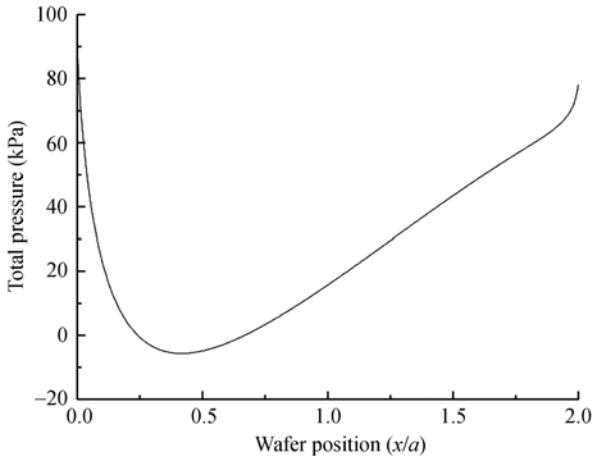


Fig. 10. Distribution of total pressure.

## 4 Conclusions

A preliminary one-dimensional contact model is put forward to describe the contact pressure and fluid pressure in CMP process wherein the deflections of the bulk pad substrate and asperities are distinguished and computed independently. The asperity deformation shapes the effectual flow clearance of the slurry fluids (there is a diverging region in the leading edge).

Contact pressure gives rise to high stress concentration at the edges, and the stress concentration is more pronounced with larger elastic constant of the asperity layer. Softer asperities will result in larger diverging region, thereby facilitating the subambient pressure value.

If the frictional shear stress is taken into consideration, enlarged diverging region will be formed and the formation of suction force will be made easier. The proposed model predicts the existence of subambient pressure and the high stress at the edges, which leads to over polishing. However, it may overestimate the effects of asperities. The model is still too simple yet, neglecting the porosity nature of the pad and the torque, and meanwhile, only one-dimensional flow is considered. Thus it only provides predictions in a quantitative sense. It is far from being satisfactory. And further improvements are needed.

**Acknowledgements** This work was supported by the National Natural Science Foundation of China (Grant No. 50390060) and College Research Fund of Beijing Jiaotong University (Grant No. 2004SM041).

## References

1 Lei H, Luo J B. CMP of hard disk substrate using a colloidal $SiO_2$ slurry: Preliminary experimental investigation. Wear, 2004, 257: 461－470 [DOI]
2 Zhang C H, Luo J B, Wen S Z. Analysis on flow properties of chemical mechanical polishing process. Lubric Eng (in Chinese), 2004, 4: 31－33
3 Xu J, Luo J B, Lu X C, et al. Progress in material removal mechanisms of surface polishing with ultra precision. Chin Sci Bull, 2004, 49(16): 1687－1693
4 Zhang C H, Luo J B, Wen S Z. Modeling chemical mechanical polishing with couple stress fluids. Tsinghua Sci Techn, 2004: 9(3): 270－273
5 Zhang C H, Luo J B, Wen S Z. Effects of nano-scale particles in chemical mechanical polishing process. Acta Phys Sinica (in Chinese), 2005, 54(5): 2123－2127
6 Hooper B J, Byrne G, Galligan S. Pad conditioning in chemical mechanical polishing. J Mater Process Techn, 2002, 123: 107－113 [DOI]
7 Levert J A, Mess F M, Salant R F. Mechanisms of chemical-mechanical polishing of $SiO_2$ dielectric on integrated circuits. Tribol Trans, 1998, 41(4): 593－599
8 Tichy J, Levert J A, Shan L, et al. Contact mechanics and lubrication hydrodynamics of chemical mechanical polishing. J Electrochem Soc, 1999, 146(4): 1523－1528 [DOI]
9 Johnson K L. Contact Mechanics. Cambridge, UK: Cambridge University Press, 1985
10 Venner C H, Lubrecht A A. Multilevel Methods in Lubrication. New York: Elsevier, 2000
11 Lei S. Mechanical interactions at the interface of chemical mechanical polishing. Dissertation for the Doctoral Degree. Georgia: Georgia Institute of Technology, 2000